Observation of an apparent first-order glass transition in ultrafragile Pt–Cu–P bulk metallic glasses

Jong H. Na[a], Sydney L. Corona[b], Andrew Hoff[b], and William L. Johnson[a,b,1]

[a]Glassimetal Technologies, Pasadena, CA 91107; and [b]Keck Laboratory of Engineering, Department of Applied Physics and Materials Science, California Institute of Technology, Pasadena, CA 91125

Contributed by William L. Johnson, December 15, 2019 (sent for review September 20, 2019; reviewed by John H. Perepezko and Frans Spaepen)

An experimental study of the configurational thermodynamics for a series of near-eutectic $Pt_{80-x}Cu_xP_{20}$ bulk metallic glass-forming alloys is reported where $14 < x < 27$. The undercooled liquid alloys exhibit very high fragility that increases as x decreases, resulting in an increasingly sharp glass transition. With decreasing x, the extrapolated Kauzmann temperature of the liquid, T_K, becomes indistinguishable from the conventionally defined glass transition temperature, T_g. For $x < 17$, the observed liquid configurational enthalpy vs. T displays a marked discontinuous drop or latent heat at a well-defined freezing temperature, T_{gm}. The entropy drop for this first-order liquid/glass transition is approximately two-thirds of the entropy of fusion of the crystallized eutectic alloy. Below T_{gm}, the configurational entropy of the frozen glass continues to fall rapidly, approaching that of the crystallized eutectic solid in the low T limit. The so-called Kauzmann paradox, with negative liquid entropy (vs. the crystalline state), is averted and the liquid configurational entropy appears to comply with the third law of thermodynamics. Despite their ultrafragile character, the liquids at $x = 14$ and 16 are bulk glass formers, yielding fully glassy rods up to 2- and 3-mm diameter on water quenching in thin-wall silica tubes. The low Cu content alloys are definitive examples of glasses that exhibit first-order melting.

glass transition | metallic glass | melting | phase transition

A liquid near its glass transition is a metastable state of matter that ultimately crystallizes given adequate time to explore its available configurational phase space. Crystallization is triggered by a relatively improbable fluctuation whereby the liquid crosses a crystal nucleation barrier. If the time required for this improbable fluctuation sufficiently exceeds the time required for the liquid to explore its available noncrystalline configurations, one may define a specific metastable configurational entropy for the liquid as $s_C = k_B \ln(W_C)$, where W_C enumerates the noncrystalline configurations per atom available. Stable liquid configurations or inherent states are defined as atomic arrangements that minimize the specific liquid configurational potential energy per atom, ϕ. Interpreting $W_C(\phi)$ as a density of inherent states (per atom) vs. ϕ leads to $s_C(\phi) = k_B \ln W_C(\phi)$ as the definition of liquid configurational entropy. Since the early work of Goldstein (1), this picture has been the basis for liquid theories based on the potential energy landscape (PEL) approach (2–7). PEL theory maintains that thermodynamic state functions (e.g., entropy, enthalpy, free energy, etc.) of a liquid are approximately separable into additive configurational and vibrational contributions that are weakly coupled via anharmonic effects (2, 3).

Defining and/or measuring $s_C(\phi)$ or $s_C(T)$ requires that the liquid explore all noncrystalline inherent states of given ϕ over the relevant experimental timescale. In short, the liquid should behave ergodically within the noncrystalline configurational phase space. Crystallization of a metastable undercooled liquid always limits the available experimental configurational equilibration time. The transformation to a fully crystallized sample involves both crystal nucleation and growth. The former is statistical, and the latter is often kinetically sluggish (8), so that progression of the liquid–crystal transformation is often spread over timescales spanning orders of magnitude (9). To further complicate measurements of $s_C(T)$, liquids near T_g relax toward equilibrium following "stretched" exponential behavior (10), where $\Delta s_C(t) \sim \exp[-(t/\tau)^\beta]$ with a stretching exponent $\beta < 1$. Typically, $\beta \sim 1/2$ or less for fragile undercooled liquids. Achieving metastable configurational equilibrium may therefore require times exceeding the Maxwell relaxation time τ_M by orders of magnitude. Configurational relaxation involves a spectrum of activated processes that include a slow α-relaxation and a fast β-relaxation. These appear to merge into a single process above a dynamic merging or crossover temperature, T_C (11, 12).

In this report, we present an experimental study of the configurational thermodynamic state functions for a series of high-fragility $Pt_{80-x}Cu_xP_{20}$ bulk metallic glass-forming liquids (13). The bulk metallic glasses form along a binary eutectic line that terminates at a ternary eutectic composition. The eutectic solid is a mixture of three crystalline phases, each having a distinct composition that differs from that of the liquid. We use this multiphase crystallized eutectic solid as a well-defined thermodynamic reference state. The crystalline eutectic solid exhibits a sharp melting transition to a homogeneous single-phase liquid at the eutectic composition and temperature, c_E and T_E, with a well-defined enthalpy and entropy of fusion.

For the metallic glasses investigated, crystal nucleation from the undercooled liquid is a transient process whereby the observed nucleation rate rises very steeply following extended configurational relaxation of the liquid over a relatively long incubation time $t_{LX}(T)$. Nucleation is followed by rapid coupled eutectic growth where the liquid-to-crystal transformation is completed in a relatively shorter timescale, $\Delta t_{LX} << t_{LX}(T)$. We show that $t_{LX}(T)$ exceeds the configurational α-relaxation time (Maxwell relaxation time), τ_α, of the liquid by orders of magnitude; typically, $t_{LX}(T)/\tau_\alpha \sim 10^3$ to 10^6. This ratio quantifies the extent of

Significance

The glass transition is ubiquitous among materials and is commonly characterized by the rapid kinetic arrest of atomic or molecular rearrangements in a liquid as temperature is lowered. The possible existence of an underlying thermodynamic phase transition has been a subject of continuing debate. Here, we present compelling evidence that the glass transition evolves into a first-order melting transition in the limit of very high-fragility metallic glass-forming liquids. These Pt-rich glasses melt in a discontinuous manner similar to melting of a crystal.

Author contributions: J.H.N. and W.L.J. designed research; J.H.N., S.L.C., and A.H. performed research; J.H.N., S.L.C., A.H., and W.L.J. analyzed data; and J.H.N., S.L.C., and W.L.J. wrote the paper.

Reviewers: J.H.P., University of Wisconsin–Madison; and F.S., Harvard University.

The authors declare no competing interest.

[1]To whom correspondence may be addressed. Email: wlj@caltech.edu.

This article contains supporting information online at https://www.pnas.org/lookup/suppl/doi:10.1073/pnas.1916371117/-/DCSupplemental.

First published January 28, 2020.

configurational equilibration of the liquid prior to the detectable onset of crystallization, and thereby the extent to which the liquid achieves metastable configurational equilibrium. The temporally sharp release of enthalpy associated with the short Δt_{LX} permits an accurate calorimetric determination of the total heat of crystallization at ambient pressure P_0 and fixed T, $h_{LX}(T,P_0,c_E)$. We argue that $h_{LX}(T,P_0,c_E)$ is an accurate measure of the liquid configurational enthalpy, i.e., that $h_C(T,P_0,c_E) \sim h_{LX}(T,P_0,c_E)$. This follows since the difference in vibrational enthalpy and entropy between the liquid and crystallized samples is observed to be quite small and essentially neglectable in bulk metallic glasses as reported recently for Cu–Zr and Al–Cu–Zr bulk glasses (14). To simplify notation, we henceforth drop ambient pressure P_0 and liquid composition c_E as independent thermodynamic variables, since both are fixed in each of our experiments, and report $h_{LX}(T)$ data.

It is common in the glass literature to measure the configurational contribution to the liquid heat capacity. For metallic glasses, this is commonly assumed to be well approximated by difference in liquid and crystal heat capacity $c_{LX}(T)$ (15–17). This heat capacity difference is often assumed to follow a "$1/T^2$" temperature dependence as originally proposed by Kubaschewski et al. (18). In PEL theory, this T dependence follows directly from assuming a Gaussian distribution of inherent states, $W_C(\phi)$ (2–4). By integrating $dh_{LX}/T = c_{LX}(T)dT/T$, one obtains a specific configurational enthalpy that follows a "$1/T$" temperature dependence with an integration constant $h_{LX}(\infty)$ representing $h_{LX}(T)$ in the limit $T \to \infty$. We describe our data using a more general empirical form for the liquid configurational enthalpy:

$$\frac{h_C(T)}{h_C(\infty)} = \left[1 - \left(\frac{\theta_h}{T}\right)^n\right], \qquad [1]$$

where θ_h is an alloy-dependent characteristic "isenthalpic" temperature and further introduce the exponent n, which takes the value $n = 1$ for the special case of a Gaussian distribution of $W(\phi)$. We refer to n as a thermodynamic fragility index. As shown in *SI Appendix*, section B), Eq. **1** is equivalent to a microcanonical configurational entropy $s_C(\phi) = k_B \ln[W_C(\phi)]$ of the following form:

$$s_C(\phi) \propto s_C(\phi_0) - C(\phi_0 - \phi)^{\frac{n+1}{n}}, \qquad [2]$$

where C is a normalization constant and ϕ_0 is the limiting value of configurational potential energy in the high T limit. For $n = 1$, the expression reduces to a Gaussian distribution for $W_C(\phi)$ (2–7).

Fitting our data yields n values spanning a surprisingly broad range, $4 < n \lesssim 50$, in stark contrast to the prediction $n = 1$ associated with a Gaussian distribution. For the ternary $Pt_{80-x}Cu_xP_{20}$ alloys, the experimental n values increase systematically with decreasing Cu content from $n \sim 4$ at $x = 27$ to $n > 13$ for $x \leq 20$. The exponent n appears to diverge and changes sign at the lowest Cu contents, $x = 14$ and 16. For such large n, the normalized configurational enthalpy, $h_C(T)/h_C(\infty)$ in Eq. **1**, approaches a Heaviside step function that abruptly jumps from 0 to 1 on passing through $T \sim \theta_h$. The glass transition approaches a first-order phase transition.

From the fits to $h_C(T) \sim h_{LX}(T)$ using Eq. **1**, we compute the specific liquid configurational entropy, $s_C(T)$, by integration. For the Pt–Cu–P alloys, we find $s_C(T) \to 0$, at a "Kauzmann" temperature (19), T_K, that lies near or even slightly above the laboratory glass transition. While the configurational entropy at T_K vanishes, the configurational enthalpy (relative to the crystallized eutectic solid) remains finite. This residual enthalpy, $h_R = h_C(T_K)$, is found to be 30 to 38% of $h_C(\infty)$ over the alloy series. For $x = 14$ and 16, the bulk glasses display a distinct latent heat and a discontinuous first-order transition at an apparent melting temperature T_{gm}. In addition to first-order melting, the $x = 14$ and 16 glasses display 1) ultrahigh Angell fragility parameter (16) $m > 90$, and non-Newtonian viscosity behavior at very low strain rates ($\sim 10^{-6}$ s^{-1}); and 2) a systematic reduction in crystal nucleation time $t_{LX}(T)$ as strain rate increases. Despite their ultrahigh fragility, the alloys at $x = 14$ and 16 form bulk glasses (>2-mm diameter glassy rods) if quenched under relatively quiescent conditions.

Results and Analysis

Table 1 lists the alloy compositions studied and summarizes important properties of the $Pt_{80-x}Cu_xP_{20}$ bulk glass-forming alloys. The crystalline alloys exhibit sharp near-eutectic melting. Instrumental broadening of the melting transition depends on the heating rate used in the differential scanning calorimetry (DSC) melting scan. This rate dependence was quantified by observing the melting transition of a pure metal (e.g., Sn) as discussed in *SI Appendix*, Fig. S7. Table 1 gives the liquidus and solidus temperatures at the lowest heating rate used for a given alloy. Based on the melting data, the composition $x = 23$ appears to be a ternary eutectic composition with a melting transition of width $\leq$4 K at a heating rate of 0.2 K/m, essentially indistinguishable from that observed for pure Sn. The binary Pt–P system displays a eutectic at the composition $Pt_{80}P_{20}$ with $T_E = 588$ °C (20). Substitution of Cu for Pt results in a binary eutectic line in the ternary system that appears to terminate at the ternary eutectic composition $Pt_{57}Cu_{23}P_{20}$, where $T_E \sim 548$ °C. The DSC melting curves taken at a commonly used heating rate of 20 K/m are shown in *SI Appendix*, Fig. S1.

The undercooled liquid alloys all display a single very sharp crystallization peak in both isothermal and constant heating rate DSC scans done throughout the temperature range from T_g to T_E. The observed glass-forming ability vs. Cu content (13) is included in *SI Appendix*, section A and Fig. S2. The bulk glasses at all compositions display an extended metastable liquid region with $T_X - T_g > 50$ K. Table 1 lists the calorimetric onset of the glass transition at 10 K/min, the measured total heat of fusion (averaged over five or more measurements) at the indicated heating rates, the measured melting onset temperature (solidus) T_S, and melting completion temperature (liquidus) T_L, both at the lowest heating rate used. Finally, the table lists the critical casting thickness, d_C, for rods of bulk glass determined by water quenching from the high temperature melt in a thin walled (1 mm) silica tube (21, 22). The d_C values provide one measure of alloy glass-forming ability that can be related to $t_{LX}(T_{nose})$; the minimum crystallization time at the "nose" of the TTT-diagram (21, 22) is discussed in ref. 21.

Fig. 1*A* shows isothermal DSC scans at different temperatures above T_g for the most extensively studied ternary eutectic $Pt_{57}Cu_{23}P_{20}$ alloy. The scans were obtained using disks (~60 to 80 mg) cut from a 2-mm glassy rod prepared by water quenching. To bring the as-cast glass samples to a well-defined initial state, all samples were first equilibrated by preannealing in the DSC at the calorimetric onset T_g (~230 °C) for 15 h. At T_g, the time for the onset of crystallization is observed to be $t_{LX}(T) > 10^6$ s (~1 wk). Following the preanneal, each sample was slowly heated at 0.5 K/min from T_g to a designated holding temperature T. Crystallization is indicated in Fig. 1*A* by a single sharp exothermic peak in the isothermal scans as plotted on a logarithmic timescale. When the exothermic peak is normalized by its height (in watts per gram) and the curves at different temperatures are shifted to align at the peak time, t_{peak}, a single peak shape vs. $\log(t/t_{peak})$ is seen (Fig. 1*B*). The plot illustrates key features of the liquid/crystal transformation: 1) there is a long incubation period $t_{LX}(T) \sim 10^4$ to 10^6 s preceding the detectable onset of exothermic heat release, 2) crystallization emerges abruptly with an exothermic signal rising sharply to a peak and then decaying rapidly, and 3) crystallization is completed over a relatively short time $\Delta t_{LX}(T) << t_{LX}(T)$. The peak time $t_{peak}(T)$ and

Table 1. Summary of basic properties of $Pt_{80-x}Cu_xP_{20}$ bulk metallic glass-forming alloys in the present study

Alloy, at.%	T_g, K, onset DSC	T_S, K, solidus (rate, K/m)	T_L, K, liquidus (rate, K/m)	Heat of fusion, J/g	Critical glass thickness, d_C, mm
$Pt_{66}Cu_{14}P_{20}$	504	828.9 (1 K/m)	879.4 (1 K/m)	67.7	1.5–2*
$Pt_{64}Cu_{16}P_{20}$	504	827.8 (1 K/m)	877.5 (1 K/m)	68.7	3
$Pt_{62}Cu_{18}P_{20}$	505	816.9 (0.5 K/m)	864.1 (0.5 K/m)	71.8	4
$Pt_{60}Cu_{20}P_{20}$	505	825.6 (1 K/m)	833.7 (1 K/m)	67.8	6–7
$Pt_{57}Cu_{23}P_{20}$ eutectic composition	505	823.8 (0.2 K/m)	827.9 (0.2 K/m)	68.5	15
$Pt_{53}Cu_{27}P_{20}$	506	819.5 (0.1 K/m)	840.1 (0.1 K/m)	67.5	27

Table includes onset of laboratory T_g at 10 K/m, melting data for solidus T_S and liquidus T_L temperatures at the indicated heating rates, heat of fusion, and the critical casting thickness (maximum rod diameter) for glass formation by water quenching in thin-wall silica tubes.

*Glass formed when quenched without mechanical agitation (see text) in a thin-wall silica capillary tube.

transformation time Δt_{LX} follow simple scaling behavior, implying a single crystallization mechanism. Fig. 1*C* shows an Arrhenius plot of $\log(t_{peak})$ vs. $1/T$, essentially a TTT-diagram for crystallization. By extrapolating the data for $\log(t_{peak})$ vs. $1/T$ to the apparent nucleation "nose" temperature of the TTT-diagram (~350 °C), one estimates a "nose time" of ~1 s. Here, nose time refers to the minimum time to crystal nucleation in the C-shaped TTT-diagram as described in ref. 22. This extrapolated time roughly agrees with that inferred from the critical casting thickness of the glass, d_C = 15 mm (Table 1) of ~1 s (22). To assess the extent of liquid configurational relaxation prior to crystallization, we carried out viscosity measurements. The viscosity data are provided in *SI Appendix*, Fig. S3. We used the viscosity data to estimate a Maxwell configurational relaxation time for the undercooled liquid, $\tau_\alpha = \eta(T)/G$, where $G \sim 32$ GPa is the shear modulus of the glass as measured ultrasonically. Fig. 1*C* compares $\log(\tau_\alpha)$ with $\log(t_{peak})$ and shows that the ratio t_{peak}/τ_α ranges from 10^3 to 10^5 as T increases above T_g. This ratio quantifies the extent of liquid relaxation toward metastable configurational equilibrium prior to crystallization. It establishes that the measured $h_{LX}(T)$ is representative of a configurationally relaxed undercooled liquid in metastable equilibrium.

To ensure the liquid/crystal transformation is completed (no glass remains) following the isothermal segment, the samples were subsequently heated (at 5 K/min) through the melting transition. For $Pt_{57}Cu_{23}P_{20}$, a relatively small heat release (~4 J/g) is consistently observed during heating in the range of 320 to 340 °C. This is believed to result from relaxation and/or coarsening of the initially crystallized structure. No other calorimetric events are observed through the eutectic melting transition. The heat of fusion was measured during each heating segment and found to have an average value of 68.5 ± 1 J/g.

High-resolution scanning electron microscopy (SEM) and chemical mapping were used to determine that the as-cast glass was chemically homogeneous on the length scale of nanometers and lacked any observable microstructure as shown in *SI Appendix*, Fig. S5. X-ray diffraction was used to establish that the as-quenched, preannealed (at T_g for 15 h), and isothermally held sample prior to the exothermic event, were all fully amorphous. A series of diffraction scans on a single 3-mm diameter disk sample were taken at various steps in the thermal history as shown in Fig. 1*D* for a sample isothermally crystallized at 240 °C. The X-ray sample was processed in the DSC to ensure its thermal history was identical to that of the other calorimetric samples. The DSC segment scans were interrupted at each respective step and the sample cooled to room temperature for X-ray. The diffraction scans indicate a fully amorphous structure for the initial as-cast sample (scan 1), the preannealed state for 15 h at 230 °C (scan 2), and the isothermally equilibrated sample at 240 °C following a holding time of 6 h and prior to the onset of the crystallization event (scan 3). Following the crystallization event after 26 h at 240 °C, the X-ray scan indicates a fully crystallized alloy (scan 4). After subsequent heating to 350 °C and holding for 2 h (scan 5), the pattern is essentially identical with scan 4. The crystalline phases produced during the exothermic event at 240 °C (scan 4) are unchanged on heating to higher temperature and following the small heat release at 320 to 340 °C. Since no new diffraction peaks are associated with the small exothermic heat release at 320 to 340 °C, the heat release in the isothermal segment at 240 °C corresponds to a transformation from a homogeneous and equilibrated undercooled liquid to a fully crystallized sample.

The total measured heat of crystallization during all isothermal segments (including the small excess contribution at ~320 to 340 °C) are compiled for reference in *SI Appendix*, Table S1. For temperatures above ~270 °C, it was not possible to carry out accurate isothermal measurements of $h_{LX}(T)$ as $t_{LX}(T)$ becomes too short to permit stabilization of the DSC control loop prior to the onset of crystallization. Data above 270 °C were acquired by preannealing the sample at 230 °C (15 h), then continuous heating at varying rates ranging from 0.1 to 10 K/min. These constant heating scans also exhibit a single very sharp crystallization event as shown in Fig. 1*E*. With increasing heating rate, crystallization occurs at progressively higher temperatures and the small exothermic heat release between 320 and 340 °C disappears, apparently merging with the single sharp exothermic event at heating rates above 1 K/min. No other detectible heat release is observed during continued heating through the eutectic melting transition. To quantify the width of the crystallization event, consider the difference between the onset and the completion temperatures. At low heating rates (below 5 K/min), the peak width is of order 2 K. The crystallization peak temperature thus accurately reflects the temperature at which the heat $h_{LX}(T)$ is released. At the highest heating rates, the exothermic peak becomes broadened and slightly shifted by instrumental effects as described in *SI Appendix*, section F and Fig. S7. Corrections for this rate-dependent peak shift are listed there (*SI Appendix*, Table S1). The constant heating rate data were combined with the isothermal data to give an $h_{LX}(T)$ curve over a broader range of T (from 230 °C up to ~290 °C) as displayed in Fig. 2*A*.

Fig. 2*A* also shows a third set of DSC results obtained by constant cooling the equilibrium melt from 900 °C, far above the liquidus temperature, and into the undercooled region below T_E (543 °C) at 10 K/min. The undercooling results were obtained using a single sample of $Pt_{57}Cu_{23}P_{20}$ cycled 40 times between 900 and 200 °C at a fixed cooling/heating rate of 10 K/min. Examples of these cyclic DSC undercooling scans are provided in *SI Appendix*, section C and Fig. S4. The sample exhibited increased undercooling with increasing number of cooling–reheating cycles. This is presumed due to dissolution of heterogeneous nucleants in the melt following repeated remelting and overheating to 900 °C. Each cycle represents roughly 2 h in real time for a total processing time (40 cycles) of roughly 3 d. The undercooling samples were unfluxed. Following repeated cycling, maximum liquid undercooling

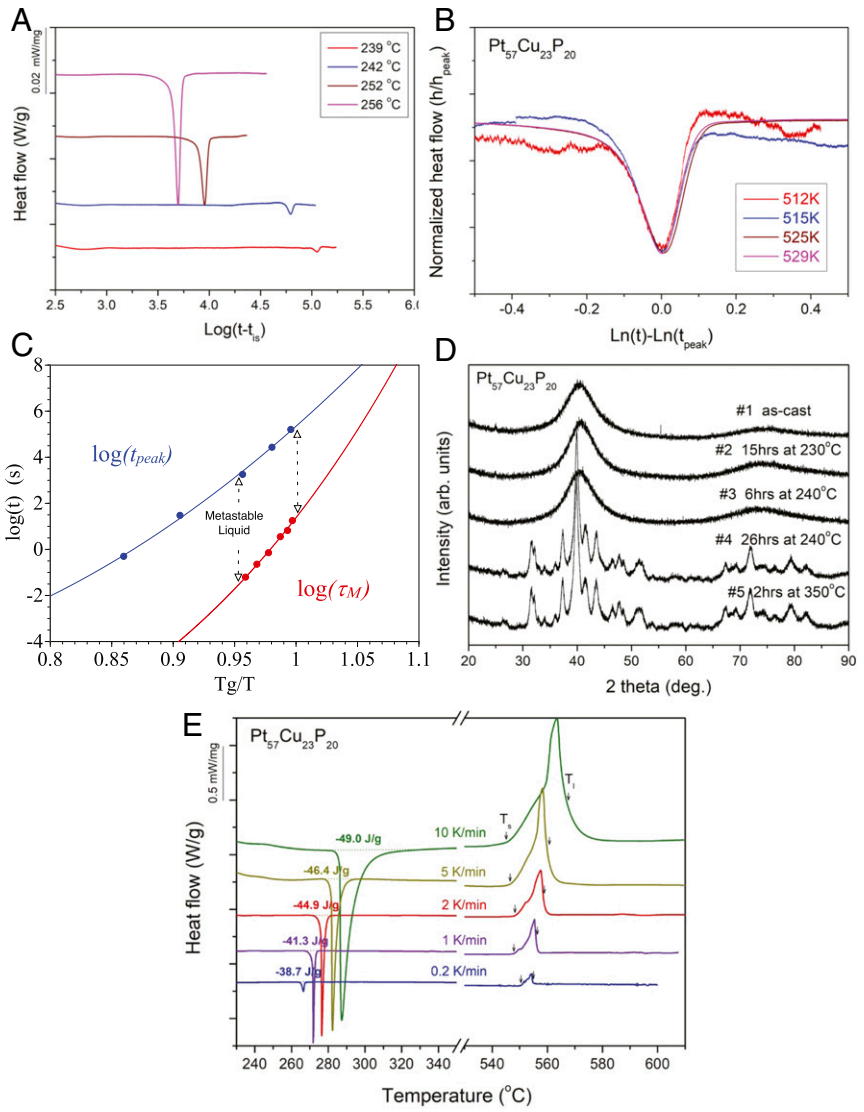

Fig. 1. (*A*) Isothermal DSC scans vs. log(t-s) at various fixed temperatures illustrating the sharp exothermic crystallization event for eutectic $Pt_{57}Cu_{23}P_{20}$. All isothermal scans were done following a preanneal of the as-cast sample for 15 h at T_g = 230 °C. (*B*) Normalized signal vs. ln(t/t_{peak}). (*C*) Plot of log(t_{peak}) vs. T_g/T compared with the logarithm of the Maxwell relaxation time, log(τ_M) = log($\eta(T)/G$) as described in the text. The vertical dashed lines indicate the configurational equilibration region. (*D*) X-ray diffraction scans of $Pt_{57}Cu_{23}P_{20}$ sample beginning in the as-cast state and at various steps employed for isothermal crystallization at 240 °C. The sample remains fully glassy prior to the exothermic heat release at 240 °C (scans 1 to 3), while it is fully crystallized following this event (scan 4). On further heating to 350 °C for 2 h (scan 5), the diffraction pattern remains essentially identical to that of scan 4. (*E*) Constant heating rate scans for $Pt_{57}Cu_{23}P_{20}$ from T_g = 230 °C through melting over a wide range of heating rates. All constant heating rate samples were preannealed for 15 h at 230 °C prior to the scan as in the isothermal scans in *A*.

to ∼365 °C (∼180 °C below T_E) was attained. The undercooling scans display a single sharp exothermic crystallization peak provided that liquid undercooling >50 K is achieved. The undercooling data provided a measure of $h_{LX}(T)$ from just above the nucleation nose to within 50 K of T_E as shown in Fig. 2*A*. Following each crystallization event, continued cooling to 200 °C resulted in no further detectable calorimetric events. The sample was then reheated through melting and back to 900 °C to complete the cycle. The heat of fusion during the reheating was measured and was repeatable with an average value of 68.5 ± 1 J/g.

Finally, Fig. 2*A* shows two additional measurements done using the rapid discharge heating (RDH) method previously described (23, 24). Here, a glassy sample rod of 4-mm diameter was heated rapidly and uniformly using ohmic dissipation at a rate of $\sim 10^5$ K/s to a target temperature and held there until crystallization occurred. The rod temperature at its center was measured using a high-speed infrared pyrometer (5-μs response time). Following rapid heating to 350 °C, the sample configurationally relaxes, and the temperature drops and stabilizes at T ∼312 °C as shown (*SI Appendix*, Fig. S8) in *SI Appendix*. Following an incubation time of $t_{LX}(T \sim 312\ °C)$ of ∼0.6 s, the sample abruptly crystallized accompanied by a sharp recalescence event and temperature rises to ∼515 °C, below but near the alloy eutectic temperature. This implies that the sample was constitutionally undercooled at 312 °C (25). A high-speed infrared video camera was employed to image the eutectic crystallization front as described in *SI Appendix*, Fig. S8. A coupled eutectic growth front propagates from a single nucleation site over the entire sample at an average speed of ∼1.5 cm/s. This eutectic growth speed is quite high [see Orava and Greer (8)]. It suggests that the short-range chemical order of the crystalline phases must already be present in the liquid, thereby mitigating

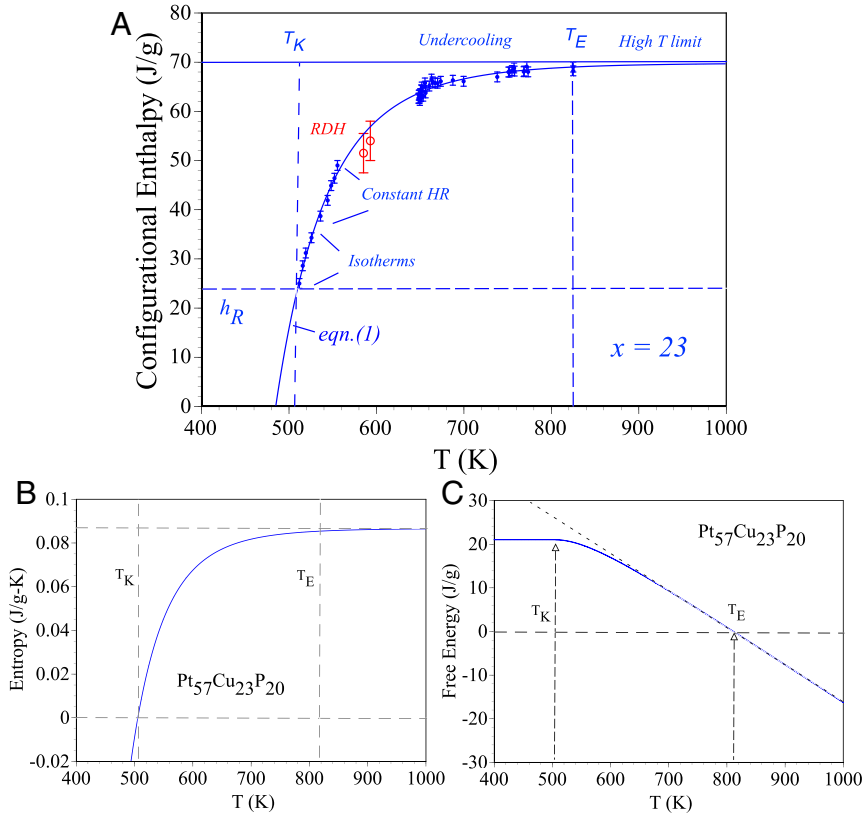

Fig. 2. (*A*) Summary of all data for heat of crystallization of $Pt_{57}Cu_{23}P_{20}$ eutectic alloy vs. *T*. Data in red were obtained by using rapid discharge heating (RDH) as described in the text. The solid is the fit obtained using Eq. **1** in the text. Fitting parameters $n = 8.04$, $\theta_h = 484$ K, and a normalization constant $h_C(\infty) = 70.2$ J/g for the high-temperature limit value are obtained. (*B*) Results of calculation of the configurational entropy $s_{LX}(T)$ using Eq. **3** showing both the Kauzmann temperature from Eq. **4** and eutectic temperature. (*C*) The configurational free energy $g_{LX}(T)$ (crystallization driving force) for $Pt_{57}Cu_{23}P_{20}$. The Turnbull linear approximation for $g_{LX}(T)$ (26) is indicated by the dotted line and provides an excellent approximation to the driving force for crystallization to deep undercooling. This indicates the configurational entropy of the liquid is nearly constant to very deep undercoolings.

the need for chemical partitioning along the advancing crystallization front. The high growth speed explains why the liquid–crystal transformation in the Pt–Cu–P alloys (at and below 312 °C) is completed in very short timescales (as in Fig. 1*E*). The temperature rise of ∼200 K on recalescence was used to estimate a heat release of $h_{LX}(312\ °C) \sim 52$ J/g as displayed in Fig. 2*A*.

The complete set of $h_{LX}(T)$ data obtained using the four different methods above are included in Fig. 2*A*. The collective data were fitted using Eq. **1** yielding fitting parameters $n = 8.04$, $\theta_h = 484$ K, and a normalization constant $h_C(\infty) = 70.2$ J/g as shown by the solid curve in the figure. The fit gives an excellent correlation of 99.8%. This fit was used to analytically compute the liquid specific configurational entropy $s_C(T)$ and specific configurational Gibb's free energy function $g_C(T)$. By integration, one obtains an expression for $s_C(T) = s_{LX}(T)$, where the integration constant is taken to be the alloy entropy of fusion $\Delta s_F(T_E)$ at the eutectic temperature T_E:

$$s_C(T) = \Delta s_F(T_E) + \int_{T_E}^{T} \frac{h_C(\infty) n \theta_h^n dT}{T^{n+2}} = \Delta s_F(T_E) - \frac{n h_C(\infty) \theta_h^n}{n+1} \left(\frac{1}{T^{n+1}}\right)\Bigg|_{T_E}^{T}. \quad [3]$$

The analytic expressions for both $s_C(T)$ and $g_C(T)$ for the Cu23 alloy are shown in Fig. 2 *B* and *C*. The entropy of fusion (Table 1) was evaluated at T_E (taken as the average of the experimental T_S and T_L). From the computed $s_C(T)$, one obtains an expression for the Kauzmann temperature T_K by setting $s_C(T_K) = 0$. Using a dimensionless Δs_F (in units of $[h_C(\infty)/\theta_h]$), T_K is given by the following:

$$T_K = \frac{T_E}{\left[1 + \left(\frac{n+1}{n}\right) \Delta s_F \left(\frac{T_E}{\theta_h}\right)^{n+1}\right]^{\frac{1}{n+1}}}. \quad [4]$$

For $Pt_{57}Cu_{23}P_{20}$, we find $T_K = 505.5$ K, very close to the calorimetric onset $T_g = 505$ K. From the $\eta(T)$ data given in *SI Appendix*, Fig. S3, the rheological glass transition temperature defined by $\eta(T_g) = 10^{12}$ Pa-s, is $T_g = 501.5$ K. The experimentally determined T_K is essentially indistinguishable from the rheologically defined laboratory T_g. From the viscosity data, an Angell fragility parameter (16) for the alloy was determined to be $m = 72 \pm 3$; the alloy is rheologically very fragile. At ambient pressure, one may ignore the "Pv" term in the configurational Gibbs free energy, i.e., $g_C(T) \sim h_C(T) - Ts_C(T)$. To calculate $g_C(T)$ in Fig. 2*C*, we assume that at T_K, the fully ordered glass configurationally freezes. Below T_K, we take $s_C(T) = 0$ and $g_C(T) = h_C(T_K)$. The apparent entropy from our fit would become negative (subensemble) below T_K, suggesting the frozen system effectively runs out of configurational states. A similar picture was introduced by Derrida (26) to describe freezing of spin glasses. Notice that $g_C(T)$ remains linear vs. *T* down to deep undercooling temperatures, thereby following the Turnbull–Spaepen approximation (27) to surprisingly high accuracy. Configurational freezing apparently sets in only at very deep liquid undercooling.

Table 2. Compilation of $Pt_{80-x}Cu_xP_{20}$ metallic-glass fitting parameters obtained from Eq. 1 for $x \geq 18$ (Eq. 5 for $x = 14, 16$), along with Angell fragility parameter m from viscosity data (*SI Appendix, Supplemental Materials*), the calculated Kauzmann temperature T_K from Eq. 4 or T_K* from Eq. 6 as described in the text, and the normalized residual configurational enthalpy, $h_R/h_C(\infty)$, for the fully ordered glass

Alloy	$h_C(\infty)$, J/g	θ_h, K	n	m fragility (Angell)	T_K(*), K	$\frac{h_R}{h_C(\infty)}$
$Pt_{66}Cu_{14}P_{20}$	67.9	561.1*	−19.2*	>90†	T_K* = 562.1	0.383
$Pt_{64}Cu_{16}P_{20}$	68.5	560.5*	−28.3*	>90†	T_K* = 560.7	0.360
$Pt_{62}Cu_{18}P_{20}$	72.4	508.3	25.7	>90†	517.4	0.360
$Pt_{60}Cu_{20}P_{20}$	68.3	492.2	13.3	>82†	511.4	0.341
$Pt_{57}Cu_{23}P_{20}$	70.2	484.8	8.36	73	505.5	0.334
$Pt_{53}Cu_{27}P_{20}$	69.9	433.6	4.30	—	472 ± 10‡	0.266

*Values obtained using Eqs. **5** and **6**. See text for discussion of fitting procedures used for samples with Cu content $x = 14, 16$.
†Viscosity is highly non-Newtonian and strain rate sensitive. Crystallization is induced by flow. It was not possible to determine an accurate value for Angell parameter m. Values given are a lower bound.
‡Value has large error due to large uncertainty in Eq. **1** fitting parameters.

Following the same methods described above for the Cu23 alloy, we determined the $h_{LX}(T)$ curves for the other metallic glasses in the $Pt_{80-x}Cu_xP_{20}$ alloy series. Both the isothermal and constant heating data for all alloys of the series are compiled for reference in *SI Appendix*, Table S1. Table 2 summarizes the fitting parameters $h_C(\infty)$, θ_h, and n obtained using Eq. **1** for $x = 18$, 20, 23, and 27. Fig. 3*A* compares $h_{LX}(T)$ plots for three representative compositions and illustrates their variation with Cu content. For the two cases $x = 14$ and 16 with the lowest Cu content, a separate discussion and analysis is given below. Table 2 includes the Kauzmann temperatures, T_K, obtained from Eq. **4**. While the computed configurational entropy of the liquids vanishes at T_K, the configurational enthalpy does not. The ordered glasses at their respective T_K possess a finite residual enthalpy $h_R = h_C(T_K)$ vs. the crystallized eutectic reference state. This residual enthalpy was evaluated using Eqs. **3** and **1**. Table 2 gives the ratio $h_R/h_{LX}(\infty)$, which varies from 0.28 to 0.36. Note that h_R represents the heat of crystallization of a fully ordered or ideal glass at T_K. The configurational enthalpy or equivalently potential energy of the ordered glass lies h_R above that of the crystalline state. Fig. 3*B* shows the overall variation of $1/n$ vs. Cu content x. The solid curve in Fig. 3*B* is a simple linear fit vs. composition and suggests that n diverges at $x \sim 17$. For reference, the X-ray diffraction data for $x = 16$ before and following crystallization and on subsequent heating are included in *SI Appendix*, section E and Fig. S6. The scans are analogous to those for the $x = 23$ case in Fig. 1*D*. As seen in Table 2, T_K increases as x decreases from $T_K = 472 \pm 10$ K at $x = 27$ to a value of $T_K = 517.4$ K at $x = 18$. For $x \leq 18$, determining T_K requires a further discussion as presented below.

The diverging n near $x \sim 17$ suggests the glass transition becomes a first-order freezing transition. On heating at a fixed rate, the calorimeter response always lags behind the measured calorimeter temperature. This lag effect was assessed and quantified by measuring the melting transition of pure Sn ($T_m = 501$ K) at heating rates varying from 0.5 to 20 K/min. The melting of Sn ($T_m = 232$ °C) was chosen for its proximity to the present temperature range of interest. The correction is described and tabulated in *SI Appendix*, Fig. S7 and Table S1. The peak shift ranges from less than ∼1 K at low heating rates up to ∼10 K at the highest heating rates. The corrected $h_{LX}(T)$ data for $x = 14$ and 16 are plotted in Fig. 4*A*. For $x = 14$, the data display a clear vertical step at a glass melting temperature of $T_{gm} = 533$ K. For $x = 16$, one observes a smaller vertical step at $T_{gm} = 548$ K. Both curves imply a latent heat and a first-order glass–liquid melting transition. For the $x = 14$ sample, we obtain a latent heat of ∼27 J/g at 533 K and T_{gm} lies ∼30 K above the nominal laboratory onset T_g. For $x = 16$, the latent heat of ∼20 J/g is somewhat smaller but occurs at a somewhat higher $T_{gm} = 547$ K.

By contrast with the $x = 20$, 23, and 27 curves in Figs. 2*A* and 3*A*, the $h_C(T)$ curves for $x = 14$ and 16 in Fig. 4*A* show opposite curvature and exhibit a clear discontinuous enthalpy jump. Below T_{gm}, one approaches the apparent first-order transition from the solid-like or "glass" side of the enthalpy discontinuity. It follows that Eq. (**1**) is no longer appropriate. Recognizing that the residual enthalpy of the glass, h_R, is an additive constant to the enthalpy of the liquid–glass freezing transition, it is natural to describe the glass below T_{gm} using a modified version of Eq. **1** that describes the approach to the discontinuity from below the step. To analyze these glass data, we introduce a power law form:

$$\frac{(h_C(T) - h_R)}{(h_C(\infty) - h_R)} = \left(\frac{T}{\theta_h}\right)^n, \qquad [5]$$

to describe the approach to melting of the glass. Notice that θ_h now represents the temperature where $h_C(T)$ for the low-temperature glass phase crosses $h_C(\infty)$, or equivalently (in the case of very large n) where $h_C(T)$ for the solid-like glass phase crosses the enthalpy of fusion of the eutectic crystalline solid. Note that the sign of n is reversed compared with the n values obtained using Eq. **1**, which describes the freezing of the liquid phase to the glass. Finally, note that $h_C(T)$ is referenced to the residual enthalpy of the ideal glass h_R, as this is the natural zero for the glass enthalpy. With increasing n, Eq. **5** describes the approach to an appropriately normalized Heaviside step function from below θ_h. Using Eq. **5** to fit the $x = 14$ and 16 data below T_{gm} gives the solid curves in Fig. 4. The fits yield very large values of the exponent; $n = -19.2$ and −29.2 for Cu14 and Cu16, respectively. The fitting parameters for $x = 14$, 16 using Eq. **5** are summarized in Table 2 together with those for $x > 16$. Using the fits from Eq. **5**, one may compute the entropy of the glass by integration of dh/T from low temperature where $s_C = 0$ to a temperature T_K* where $s_C(T_K^*) = \Delta s_F$, the entropy of fusion of the crystallized eutectic. T_K* is now an "inverse" Kauzmann temperature, i.e., the temperature where the glass configurational entropy equals the entropy of fusion of the crystalline eutectic alloy. The analytic expression for T_K* is as follows:

$$T_K^* = \theta_h \left[\frac{(n-1)(h_C(\infty) - h_R)\theta_h}{n h_C(\infty) T_E}\right]^{1/(n-1)}. \qquad [6]$$

T_K* is effectively an upper bound for the glass melting temperature. Note that T_K* for the $x = 14$ alloy is slightly lower than for $x = 16$, implying a more restrictive upper bound.

The data for Cu14 (Cu16) compositions in the glass region below $T_{gm} = 533$ K (546 K) are generally obtained from isothermal crystallization scans. The glass enthalpy approaches a residual value of $h_R \sim 26.0$ J/g (24.5 J/g). The T dependence of the glass enthalpy below T_{gm} suggests that the equilibrium glass is in a configurationally excited state. While slow kinetics could limit relaxation and equilibration of the glass below T_{gm}, this seems unlikely as the data were obtained under isothermal conditions whereby the glass relaxes for timescales far exceeding the configurational Maxwell relaxation time as discussed earlier. Assuming the data represent a glass in configurational equilibrium, one may use the enthalpy fits from Eq. **5** to compute the T-dependent configurational entropy of the glass below T_{gm}. Combining the fits with the measured latent heat of glass melting at T_{gm} and the measured entropy of fusion of the crystalline eutectic, one may generate a piecewise continuous configurational $s_C(T)$ plot for the glass/liquid system as displayed in Fig. 4*B*. The figure shows the configurational entropy vs. T (entropy

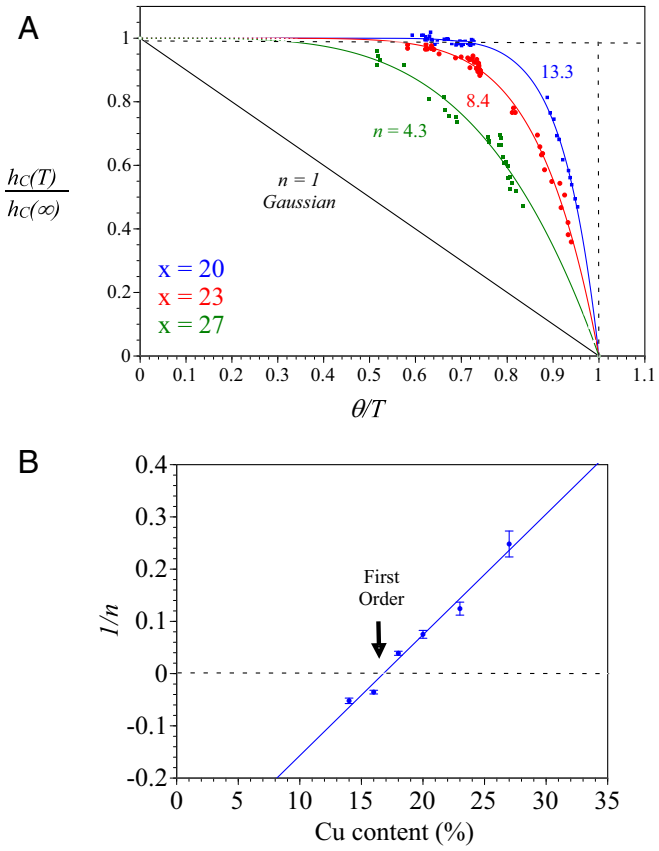

Fig. 3. (*A*) Plot of dimensionless configurational enthalpy data [$h_C(T)/h_C(\infty)$] vs. dimensionless temperature, θ/T, for alloys with Cu contents x = 27, 23, and 20 (*Left* to *Right*) as described in the text. The curves illustrate evolution of the glass transition toward a first-order phase transition with decreasing Cu content. The black line shows prediction for a Gaussian density of inherent states. The solid curves (green, red, and blue) are fits using Eq. **1**. (*B*) Variation of the effective glass transition width, n^{-1}, vs. Cu content for all samples (see text for discussion of Cu14 and Cu16 cases).

in units of the gas constant R) for both the x = 14 and 16 glass–liquid systems. Within the accuracy of the Eq. **5** and assumption of configurational equilibrium, for x = 14 one finds the configurational entropy at T_{gm} = 533 K to be 0.0308 J/g-K or 0.533 R. The Eq. **5** fit then provides an extrapolation of the glass entropy from T_{gm} to T = 0 K. The predicted entropy at T = 0 K vanishes within an uncertainty of approximately ±0.03 R; and $s_C(T)$ obeys the third law of thermodynamics within the stated uncertainties. This resolves Kauzmann's apparent paradox. The equilibrium glass configurational entropy never becomes negative but instead rapidly approaches that of the crystallized eutectic solid as T falls below T_{gm}. In this respect, the glass behaves much like a crystalline solid but with a relatively smaller heat of formation for configurational excitations (or defects in the case of crystals).

It should be noted that we have ignored possible vibrational contributions to the entropy throughout our analysis. In fact, our data for the heat of crystallization implicitly include any contribution arising from differences in anharmonicity between the glass and crystalline eutectic since we measure the total heat release during crystallization. In this regard, the form of Eq. **5** and the high values of the exponent n obtained strongly suggest that anharmonic contributions are relatively small. This follows since anharmonicity, to leading order in T, would display a "T^2" contribution to the heat of crystallization. This contrasts sharply with the large values of n indicated from fitting the data. Configurational degrees of freedom must therefore dominate the T dependence of $h_C(T)$ below T_{gm}. The ordered glass might be usefully viewed as a configurationally ordered solid, albeit with an infinite unit cell. It should not be surprising that this configurationally ordered glass has a unique configurational ground state enthalpy, h_R, that differs from the eutectic crystalline solid state. Allotropic or polymorphic crystalline phases also have characteristic ground state energies that differ by phase.

Discussion and Summary

The $Pt_{80-x}Cu_xP_{20}$ bulk metallic glass-forming alloys investigated are unique in several respects. The undercooled homogeneous liquid crystallizes in a single sharp step by coupled eutectic growth producing a well-defined crystallized reference state. This enables an accurate direct measurement of the liquid enthalpy referenced to the crystallized eutectic solid. The onset of crystallization follows a relatively long incubation time $t_{LX}(T)$ that far exceeds the Maxwell relaxation time $\tau_M(T)$ of the liquid by orders of magnitude as seen in Fig. 1*C*. The liquid undergoes extensive configurational relaxation, thereby achieving metastable equilibrium prior to the onset of crystallization. These features enable accurate assessment of the metastable equilibrium configurational enthalpy of the liquid as referenced to the crystalline eutectic state.

The T dependence of the $h_C(T)$ curves differs dramatically from that expected for a conventional glass having a Gaussian distribution $W(\phi)$ of inherent configurational states where n = 1. According to Eq. **2**, the large and increasing n values obtained as Cu content decreases imply a microcanonical density of configurational inherent states that approaches simple exponential behavior of the form $W(\phi) \sim e^{K\phi}$ vs. configurational potential energy ϕ. The large n values imply a diverging heat capacity, $c_{LX}(T) = nh(\infty)/\theta_h$ at $T = \theta_h$, as n increases. Equivalently, the glass transition approaches a first-order melting transition as $n^{-1} \to 0$. At x = 14 and 16, Eq. **1** fails to provide a suitable description of the data since the curvature of the $h_C(T)$ changes sign. For these cases, we introduced Eq. **5** instead to describe the equilibrium configurational excitation of the solid glass phase as it approaches melting at T_{gm}. By analogy to Eq. **2**, it is straightforward to show Eq. **5** is also equivalent to a microcanonical density of configurational states of the form $W(\phi) \sim \exp[\phi^{(n-1)/n}]$. Within measurement capability, we observe a latent heat of melting at a well-defined T_{gm} for the x = 14 and 16 samples. This signals unambiguous first-order melting. The glasses apparently melt in a similar manner to a crystal, but very differently than expected for a traditional glass transition. The ordered glasses melt to a fully disordered liquid in its high temperature limit. Finally, the equilibrium glass configurational entropy remains positive and finite below T_{gm} and approaches zero in the limit of low T. The Kauzmann paradox is averted, and the configurational entropy contribution appears to obey the third law.

Based on molecular dynamic (MD) simulations, Berthier and coworkers (28, 29) and others (30) have recently reported that ultrastable (configurationally relaxed) atomic glasses with a polydisperse atomic size distribution exhibit first-order melting behavior on rapid heating through the glass transition. Such ultrastable glasses are prepared experimentally (and in simulations) using layer-by-layer atomic deposition onto substrates held near T_g, thereby allowing a degree of configurational relaxation not achievable on cooling a monolithic liquid (28, 29). In the MD simulations, such glasses melt by propagation of a first-order melting front in the same manner as crystals melt. The authors attribute this first-order melting behavior to the highly ordered, low configurational enthalpy state associated with the ultrastable glasses. In the ultrafragile Pt–Cu–P alloys, we have shown that extensive configurational relaxation of the liquid state is achieved near T_{gm} prior to the onset of crystallization. We thereby achieve a low enthalpy "ideal-glass" state of zero configurational entropy lying near the lowest achievable glass enthalpy $h_C(T) = h_R$. We suggest that the

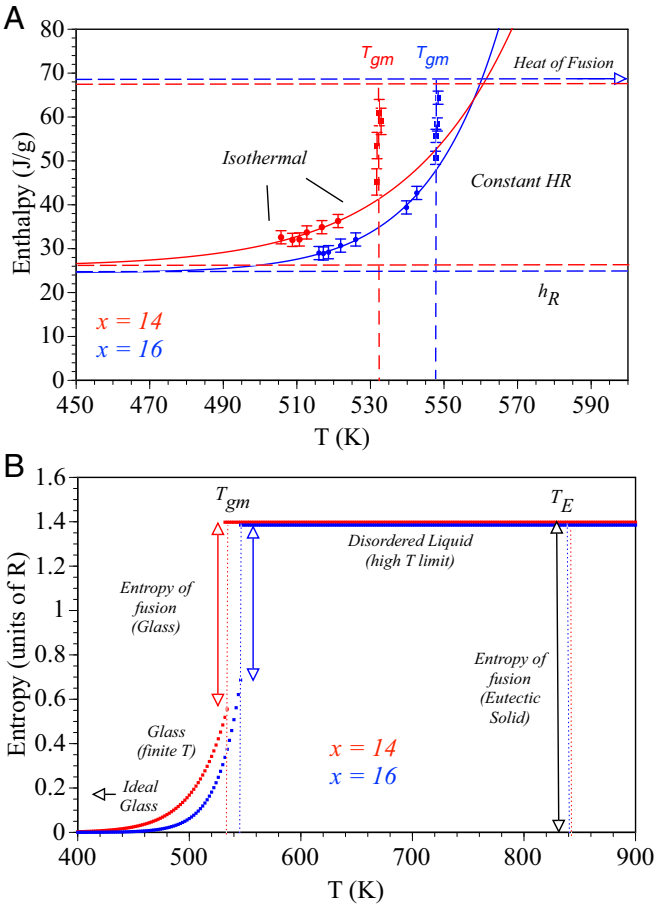

Fig. 4. (*A*) Configurational enthalpy vs. *T* for Cu14 and Cu16 glasses initially annealed (3 h) at the laboratory T_g (501 K). Plot illustrates the first-order glass melting transition at T_{gm} (see text for discussion), and the vertical lines illustrate the transition temperature and magnitude of the latent heat of glass–liquid melting. The dotted lines are the fits to the isothermal low temperature data using Eq. **5** as described in the text. The glasses near T_g exhibit a residual enthalpy of $h_R = 24.8$ J/g for Cu16 and 26 J/g for Cu14 with respect to the equilibrium crystallized sample. (*B*) Calculated configurational entropy (in units of the gas constant R) for Cu14 and Cu16 using the fitting parameters from Eq. **5**. The figure displays the entropy of fusion of the glasses at $T_{gm} = 533$ K (Cu14) and $T_{gm} = 548$ K (Cu16) computed from the latent heat of glass melting. Below T_{gm}, the computed entropy of the glasses decreases rapidly as described by a power law with exponent $n = 18.2$ (Cu14) and $n = 27.3$ (Cu16). The entropy vanishes only in the low temperature limit. As such, the configurational entropy of the glasses apparently obeys the third law of thermodynamics, thereby avoiding the Kauzmann paradox where the configurational entropy would become negative.

first-order transition at T_{gm} is analogous to that seen in the ultrastable glasses in MD simulations.

If we consider alloy composition x to a tunable external parameter, then our results lead to a picture wherein the configurational entropy of the undercooled liquids $s_C(T,x)$ develops a folding behavior vs. T at a critical value of $x_c \sim 16$ to 17. The $s_C(T,x)$ isobars become folded when $x < x_c$ giving rise to an entropy of glass fusion. At x_c, one expects a critical point as $1/n \rightarrow 0$ accompanied by diverging heat capacity. Below x_c, the glass transition is first order with a progressively increasing latent heat as x decreases. This picture is reminiscent of Van der Waal's description of the liquid/gas transition where the P-v isotherms become folded below the liquid–gas critical temperature. In the present case, x correlates directly with liquid fragility. Essentially, liquid fragility plays the role of an externally tunable control parameter. The first-order glass transition is associated with the ultrahigh fragility limit. The rheological Angell fragility parameter m is also expected to diverge, and liquid viscosity should show a discontinuous jump at T_{gm}. It is noteworthy that such behavior has been reported in bulk metallic glass-forming liquids (e.g., Vitreloy 1) well above the laboratory T_g (31, 32). For the van der Waal's picture of the liquid–gas transition, the liquid bulk modulus vanishes at a critical point. The authors suggest the present first-order glass transition be interpreted as a transition from a fluid lacking long-range elasticity to a solid with a finite quasistatic macroscopic shear modulus.

To conclude, we comment on why the present Pt–Cu–P glasses display such unusual first-order freezing/melting behavior. Equivalently, one may question the microscopic origins of liquid fragility. If the glass transition is connected with the emergence of long-range elastic rigidity, one may speculate that the present liquids lack inherent local rigidity. A lack of local rigidity of atomic clusters can be traced to a soft interatomic potential that provides little resistance to bond length changes and therefore to configurational rearrangements of the atomic cluster. This leads naturally to a narrow distribution of inherent states and thereby to a low freezing temperature. The onset of long-range elasticity is accompanied by long-range elastic interactions, of the type discussed by Eshelby (33, 34), that broaden the configurational excitation spectrum on freezing. If elastic percolation in three dimensions is inherently a first-order transition, this will lead to a sharp glass transition. We speculate that the noble metals Pt and Cu and particularly P are characterized by soft interatomic interactions that lead to a narrow PEL at high T, which then broadens substantially with the onset of long-range elastic rigidity during freezing at low T. The relatively low freezing temperature (T_g) of the present Pt–Cu–P glasses by comparison with other similar transition metal–metalloid glasses provides a clue supporting this conjecture.

Experimental Methods

The calorimetry work reported here was done using calibrated Netzsch 404C F3 DSC with separate calibrations for each constant heating rate reported. A sapphire standard is used for calibration. X-ray diffraction scans were acquired using a Bruker D2 Phaser diffractometer. Viscosity measurements were carried out using a Perkin-Elmer Thermo Mechanical Analyzer in the beam-bending configuration. The RDH experiments were performed using 15-kJ capacitive discharge heating system as described in ref. 23. The system permits rapid and very uniform heating of rods of diameter $d = 3$ to 5 mm and length $L = 3$ cm at heating rates ranging up to $\sim 10^5$ K/s. The reader is referred to ref. 23 for details. For rapid heating experiments, temperatures were measured using a noncontact high-speed Impac series 5 infrared pyrometer with 5-μs time resolution. A FLIR SC-4000 infrared camera (having 256,000 pixels, frame rates up 1,300 frames/s) was employed in conjunction with the RDH system to provide the infrared images of coupled-eutectic crystallization of rapidly heated glassy rods. Ultrasonic elastic constant measurements were done using the pulse-echo method with 25-MHz quartz transducers to determine shear and longitudinal sound velocities on 3-mm-diameter glassy rods. Density measurements were done using the Archimedes method.

To measure the heat of crystallization for a configurationally equilibrated liquid, the crystallization time t_{LX} must exceed the time required for liquid relaxation. Time-dependent c_P studies (35–37) show that this may require up to 10^3 α-relaxation steps of duration τ_α = Maxwell relation time = η(T)/G to ensure the liquid reaches metastable equilibrium. In the present work, this requires $t_{LX} > 10^3$ to 10^5 τ_α. Following the onset of crystal nucleation, the liquid–crystal transition occurs in a single step by rapid coupled eutectic growth (7, 8, 38, 39) leading to a small Δt_{LX}. At higher T (e.g., Fig. 2*A*, RDF data at 312 °C), we used high-speed infrared imaging to directly measure the speed of eutectic crystallization front to be ~1.5 cm/s (*SI Appendix*, Fig. S8). This high speed explains the small scale of Δt_{LX} seen in calorimetry. To accurately measure h_{LX}, the calorimetric power signal generated by the liquid-to-crystal transformation $\Delta P_{LX}(t) \sim h_{LX}/\Delta t_{LX}$ must lie above the sensitivity level of the instrument. The sensitivity/stability of the Netzsch 404 was determined to be roughly ±10 to 15 μW. At the lowest temperatures (longest

Δt_{LX}), calorimeter noise and drift limit accuracy as can be seen, for example, in Fig. 1*A* for the lowest isothermal temperatures (e.g., 239 °C).

Data Availability. All data used in the paper are compiled in *SI Appendix*. *SI Appendix*, Table S1 lists all data for the isothermal and constant heating rate experiments.

ACKNOWLEDGMENTS. We acknowledge the NSF for partial support of the present work under Grant DMR-1710744 and support of S.L.C. under the NSF Graduate Research Fellowship Program (Grant DGE-1144469). We acknowledge Prof. Jorg Loffler of Eidgenössische Technische Hochschule Zürich for providing the high-resolution SEM images and chemical analysis included in *SI Appendix, Supplemental Materials*.

1. M. Goldstein, Viscous liquids and glass transition—a potential energy barrier picture. *J. Chem. Phys.* **51**, 3728–3739 (1969).
2. F. H. Stillinger, P. G. Debenedetti, Glass transition thermodynamics and kinetics. *Ann. Rev. Condens. Matter Phys.* **4**, 263–285 (2013).
3. P. G. Debenedetti, F. H. Stillinger, Supercooled liquids and the glass transition. *Nature* **410**, 259–267 (2001).
4. F. Sciortino, W. Kob, P. Tartaglia, Inherent structure entropy of supercooled liquids. *Phys. Rev. Lett.* **83**, 3214–3217 (1999).
5. L. M. Martinez, C. A. Angell, A thermodynamic connection to the fragility of glass-forming liquids. *Nature* **410**, 663–667 (2001).
6. D. J. Wales, *Energy landscapes: Applications to Clusters, Biomolecules, and Glasses* (Cambridge University Press, 2004), chap. 10.
7. T. F. Middleton, D. J. Wales, Energy landscapes of some model glass formers. *Phys. Rev. B* **64**, 024205 (2001).
8. J. Orava, A. L. Greer, Fast and slow crystal growth kinetics in glass-forming melts. *J. Chem. Phys.* **140**, 214504 (2014).
9. J. Malek, Kinetic analysis of crystallization processes in amorphous materials. *Thermochim. Acta* **355**, 239–253 (2000).
10. G. Williams, D. C. Watts, Non-symmetrical dielectric relaxation behavior arising from a simple empirical decay function. *Trans. Faraday Soc.* **66**, 80–85 (1970).
11. G. P. Johari, M. Goldstein, Viscous liquids and the glass transition. II. Secondary relaxations in glasses of rigid molecules. *J. Chem. Phys.* **53**, 2372–2388 (1970).
12. H. B. Yu, W. H. Wang, H. Y. Bai, K. Samwer, The beta-relaxation in metallic glasses. *Natl. Sci. Rev.* **1**, 429–461 (2014).
13. J. H. Na *et al*., "Bulk Pt-Cu-P glasses bearing Ag, B, and Au," US Patent 10,036,087 (2018).
14. H. L. Smith *et al*., Separating the configurational and vibrational entropy contributions in metallic glasses. *Nat. Phys.* **13**, 900–905 (2017).
15. S. C. Glade, R. Busch, D. S. Lee, W. L. Johnson, Thermodynamics of Cu-Ti-Zr-Ni, Zr-Cu-Ni-Al-Ti, and Zr-Cu-Ni-Al-Nb bulk metallic glass forming alloys. *J. Appl. Phys.* **87**, 7242–7248 (2000).
16. L.-M. Wang, C. A. Angell, R. Richert, Fragility and thermodynamics in nonpolymeric glass-forming liquids. *J. Chem. Phys.* **125**, 074505 (2006).
17. R. Busch, Y. J. Kim, W. L. Johnson, Thermodynamics and kinetics of the undercooled liquid and the glass transition of the Zr-Ti-Cu-Ni-Be alloy. *J. Appl. Phys.* **77**, 4039–4043 (1995).
18. O. Kubaschewski, C. B. Alcok, P. J. Spencer, *Materials Thermochemistry* (Pergamon, New York, ed. 6, 1993).
19. W. Kauzmann, The nature of the glassy state and the behavior of liquids at low temperature. *Chem. Rev.* **43**, 219–256 (1948).
20. P. Villars, H. Okamoto, and P. Cenzual, Eds. "Pt-P binary phase diagram" in *ASM Alloy Phase Diagram Online Data Base* (ASM International, 2018).
21. W. L. Johnson, J. H. Na, M. D. Demetriou, Quantifying the origin of metallic glass formation. *Nat. Commun.* **7**, 10313 (2016).
22. J. H. Na *et al*., Compositional landscape for glass formation in metal alloys. *Proc. Natl. Acad. Sci. U.S.A.* **111**, 9031–9036 (2014).
23. W. L. Johnson *et al*., Beating crystallization in glass-forming metals by millisecond heating and processing. *Science* **332**, 828–833 (2011).
24. G. Kaltenboeck *et al*., Accessing thermoplastic processing windows in metallic glasses using rapid capacitive discharge. *Sci. Rep.* **4**, 6441 (2014).
25. W. J. Boettinger, U. R. Kattner, K.-W. Moon, J. H. Perepezko, "DTA and heat-flux DSC measurements of alloy melting and freezing" in *Methods for Phase Diagram Determination*, J. C. Zhao, Ed. (Elsevier, 2007), chap. 5, pp. 151–221.
26. B. Derrida, Random-energy model: An exactly solvable model of disordered systems. *Phys. Rev. B* **24**, 2613–2626 (1981).
27. C. V. Thompson, F. Spaepen, On the approximation of the free energy change on crystallization. *Acta Metall.* **27**, 1855–1859 (1979).
28. R. L. Jack, L. Berthier, The melting of stable glasses is governed by nucleation-and-growth dynamics. *J. Chem. Phys.* **144**, 244506 (2016).
29. L. Berthier, M. D. Ediger, Facets of glass physics. *Phys. Today* **69**, 40–46 (2016).
30. E. Flenner, L. Berthier, P. Charbonneau, C. J. Fullerton, Front-mediated melting of ultra-stable glasses. arXiv:1903.09108 (3 October 2019).
31. C. Way, P. Wadhwa, R. Busch, The influence of shear rate and temperature on the viscosity and fragility of the Zr41.2Ti13.8Cu12.5Ni10.0Be22.5 metallic-glass-forming liquid. *Acta Mater.* **55**, 2977–2983 (2007).
32. J. J. Z. Li, W. K. Rhim, C. P. Kim, K. Samwer, W. L. Johnson, Evidence for a liquid-liquid phase transition in metallic fluids observed by electrostatic levitation. *Acta Mater.* **59**, 2166–2171 (2011).
33. J. D. Eshelby, The elastic field outside an ellipsoidal inclusion. *Proc. R. Soc. Lond. Ser A Math. Phys. Sci.* **252**, 561–569 (1959).
34. J. D. Eshelby, "The continuum theory of lattice defects" in *Solid State Physics—Advances in Research and Applications*, F. Seitz, D. Turnbull, Eds. (Academic Press, San Diego, CA), vol. **3**, pp. 79–144 (1956)
35. N. O. Birge, Specific-heat spectroscopy of glycerol and propylene glycol near the glass transition. *Phys. Rev. B Condens. Matter* **34**, 1631–1642 (1986).
36. Y. H. Jeong, I. K. Moon, Ergodic-nonergodic glass transition and enthalpy relaxation of a supercooled liquid. *Phys. Rev. B Condens. Matter* **52**, 6381–6385 (1995).
37. C. C. Yu, H. M. Carruzzo, Frequency dependence and equilibration of the specific heat of glass-forming liquids. *Phys. Rev. E Stat. Nonlin. Soft Matter Phys.* **69**, 051201 (2004).
38. R. Trivedi, P. Magnin, W. Kurz, Theory of eutectic growth under rapid solidification conditions. *Acta Metall.* **35**, 971–980 (1987).
39. D. M. Herlach, Non-equilibrium solidification of undercooled metallic melts. *Mater. Sci. Eng. R Rep.* **12**, 177–272 (1994).